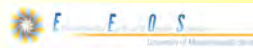


Microphytobenthos (end)

Class 7: Tu September 23, 2008



Conclusions on microphytobenthos

- Microphytobenthic production is often a major source of labile organic matter in shallow benthic systems from the intertidal to approximately the 1% light depth (or slightly deeper)
- Mucus production can have profound effects on sediment transport and organic geochemistry
- Microphytobenthic production is intimately coupled to the physics of the benthic boundary layer
- It can be measured using ^{14}C , O_2 , or fluorescence
- Benthic diatom specific growth is often very slow

Slide 1 Conclusions on microphytobenthos

NOTES:

Class schedule

Order of topics

- Today: Finish of benthic diatoms
- Thursday: Benthic community structure
 - overview of benthic community structure, including benthic population processes
 - Tools of the trade: alpha, beta & gamma diversity
 - Gallagher, E. D., G. B. Gardner and P. A. Jumars. 1990. Competition among the pioneers in soft bottom benthic succession: field experiments and analysis of the Gilpin-Ayala competition model. *Oecologia* 83: 427-442.
 - Whittatch, R. B. 1980. Patterns of resource utilization and coexistence in marine intertidal deposit-feeding communities. *J. Mar. Res.* 38: 743-765.
 - Gallagher & Keay (1998)
-



Slide 2 Microphytobenthos (end)

NOTES:

Slide 3 Class schedule

NOTES:

Microphytobenthic production (end)

Benthic boundary layers, Revsbech & Jørgensen (1983) O₂ method and PAM fluorescence



Serôdio & Catarino (2000)

O₂ microelectrodes & pulse amplitude modulated (PAM) fluorescence, diver-PAM, <http://www.walz.com/>

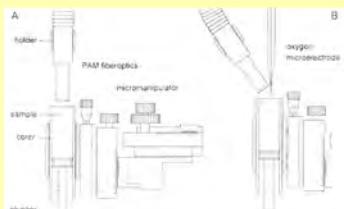


Fig. 1. The setup used for (A) measuring chl *a* fluorescence, using a PAM fluorometer, and for (B) measuring photosynthesis, using oxygen microelectrodes, on undisturbed microphytobenthic samples. When measuring photosynthetic rates, the PAM fiberoptics is used to illuminate the sample surface.

Jørgensen & Revsbech (1985)

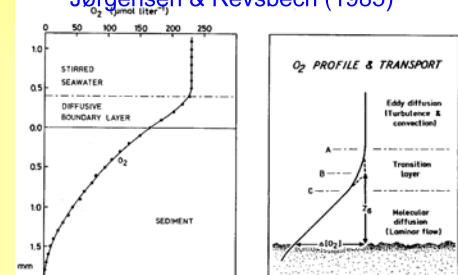


Fig. 1. Left. Oxygen microprofile in sediment collected from Aarhus Bay at 20-m water depth, July 1982. A transition (broken line) is seen above the sediment surface between the stirred seawater with homogeneous O₂ distribution and the diffusive boundary layer with a steep O₂ gradient. Right. The boundary layer at the sediment surface as defined by chemical transport processes and gradients. The oxygen microgradients are here used to define the outer limit (A) of the diffusive boundary layer as well as the true (C) and the effective (B) diffusive boundary layer.

Slide 4 Microphytobenthic production (end)

NOTES:

Slide 5 Serôdio & Catarino (2000)

NOTES:

Slide 6

NOTES:

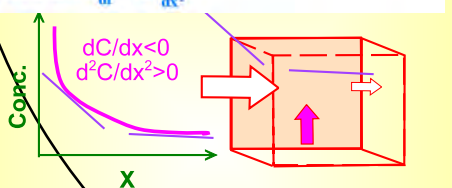
<p>Benthic boundaries</p> <p>Ekman layer</p> <p>Log layer</p> <p>Viscous sublayer</p> <p>Molecular diffusive sublayers</p> <p>Ox c zone</p> <p>Ox d zed zone</p> <p>Sulfidogenic zone</p> <p>Methanogenic zone</p>	<p>Slide 7</p> <p>NOTES:</p>																																
<p>Thicknesses of benthic boundaries</p> <table border="1"> <thead> <tr> <th>Parameter</th> <th>Deep-Sea</th> <th>Shelf</th> <th>Description</th> </tr> </thead> <tbody> <tr> <td>U (cm/s)</td> <td>3</td> <td>30</td> <td>average water velocity</td> </tr> <tr> <td>U_s (cm/s), boundary shear velocity</td> <td>0.1</td> <td>1</td> <td>Boundary shear velocity (the square root of boundary shear stress/sea water density)</td> </tr> <tr> <td>ν (cm/s)</td> <td>2</td> <td>200</td> <td>characteristic eddy viscosity</td> </tr> <tr> <td>z_e (cm)</td> <td>500</td> <td>5000</td> <td>Ekman depth</td> </tr> <tr> <td>z_l (cm)</td> <td>100</td> <td>1000</td> <td>log layer thickness</td> </tr> <tr> <td>z_v (cm)</td> <td>2</td> <td>0.2 to 1</td> <td>viscous sublayer thickness</td> </tr> <tr> <td>z_d (cm)</td> <td>0.2</td> <td>0.02-0.1</td> <td>diffusive sublayer thickness $z_d = \frac{\nu}{\mu} \cdot \frac{1}{S_a}$, where S_a = Schmidt number $\approx 5 \pm 0.00$ for O₂ or CO₂ μ = molecular diffusivity</td> </tr> </tbody> </table>		Parameter	Deep-Sea	Shelf	Description	U (cm/s)	3	30	average water velocity	U_s (cm/s), boundary shear velocity	0.1	1	Boundary shear velocity (the square root of boundary shear stress/sea water density)	ν (cm/s)	2	200	characteristic eddy viscosity	z_e (cm)	500	5000	Ekman depth	z_l (cm)	100	1000	log layer thickness	z_v (cm)	2	0.2 to 1	viscous sublayer thickness	z_d (cm)	0.2	0.02-0.1	diffusive sublayer thickness $z_d = \frac{\nu}{\mu} \cdot \frac{1}{S_a}$, where S _a = Schmidt number $\approx 5 \pm 0.00$ for O ₂ or CO ₂ μ = molecular diffusivity
Parameter	Deep-Sea	Shelf	Description																														
U (cm/s)	3	30	average water velocity																														
U_s (cm/s), boundary shear velocity	0.1	1	Boundary shear velocity (the square root of boundary shear stress/sea water density)																														
ν (cm/s)	2	200	characteristic eddy viscosity																														
z_e (cm)	500	5000	Ekman depth																														
z_l (cm)	100	1000	log layer thickness																														
z_v (cm)	2	0.2 to 1	viscous sublayer thickness																														
z_d (cm)	0.2	0.02-0.1	diffusive sublayer thickness $z_d = \frac{\nu}{\mu} \cdot \frac{1}{S_a}$, where S _a = Schmidt number $\approx 5 \pm 0.00$ for O ₂ or CO ₂ μ = molecular diffusivity																														
<p>Revsbech & Jørgensen (1983)</p> <p>O₂ microelectrode profiles of the best methods for estimating benthic primary production</p> <p>Primary production of sediments</p> <p>Fig. 3. Recorder output showing three oxygen profiles. The first profile was obtained in the light with 300 lux/cm⁻² and one oxygen profile was recorded after 1 min in the dark. Recorder was stopped between profile measurements.</p> <p>Oxygen profiles in AB sediment due to illumination with a light of 300 lux⁻² and the time interval in the dark. The difference between the two was used to calculate primary production. Curves were drawn from data in Fig. 2.</p> <p>O₂ primary production obtained by subtracting the integrated light & dark profiles (after 1 min in dark)</p> <p>E.O.S. University of Münster/Geest</p>																																	
<p>Slide 8 Thicknesses of benthic boundaries</p> <p>NOTES:</p>																																	
<p>Slide 9 Revsbech & Jørgensen (1983)</p> <p>NOTES:</p>																																	

Advection-diffusion equation

Fick's First & Second Laws

$$0 = \frac{\partial C}{\partial t} - u \frac{\partial C}{\partial x} - v \frac{\partial C}{\partial y} - w \frac{\partial C}{\partial z} + K_x \frac{\partial^2 C}{\partial x^2} + K_y \frac{\partial^2 C}{\partial y^2} + K_z \frac{\partial^2 C}{\partial z^2} + R_c$$

Fick's 1st Law: $J_x = -D \frac{dC}{dx}$,
Fick's 2nd Law: $\frac{dC}{dt} = D \frac{d^2 C}{dx^2}$,



Slide 10 Advection-diffusion equation

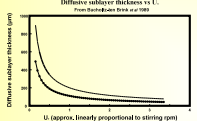
NOTES:

Stirring effects on diatom production

Stirred 0.23 d⁻¹ (3-d doubling), Unstirred 0.14 d⁻¹ (6 d)

Table 3. Results of stirred vs. unstirred incubation of mixed field populations collected 3 August 1987. SD in parentheses ($n = 3$). Units given in Table 1.

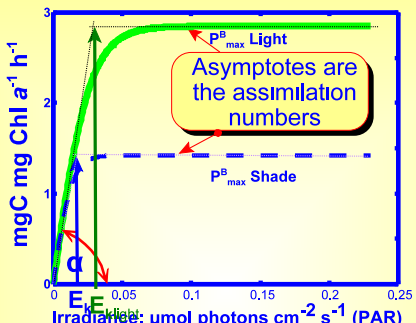
	A^* ($\times 10^3$)	I^* ($\times 10^3$)	R^*	SC	C_D ($\times 10^3$)	μ
Stirred	16.87(2.17)	1.41	764(43)	75(5)	4.16(0.82)	0.23(0.02)
Unstirred	10.62(0.19)	1.34	356(32)	47(1)	5.62(0.67)	0.11(0.02)



Slide 11 Stirring effects on diatom production

NOTES:

Chl a-specific gross productivity

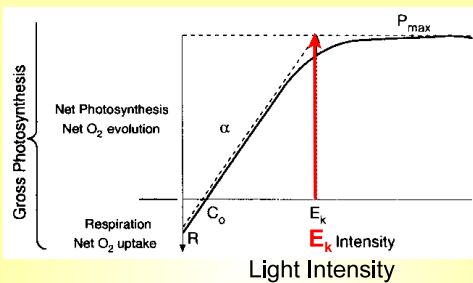


Slide 12

NOTES:

Falkowski & Raven P vs. E curves

Falkowski & Raven (1997, p. 196, Fig 7.2)

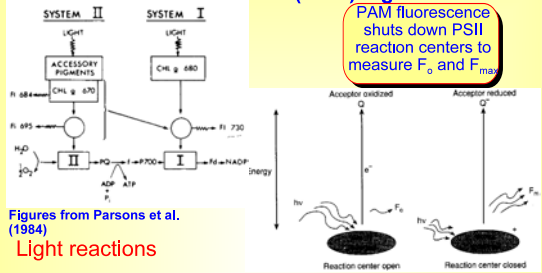


Slide 13 Falkowski & Raven P vs. E curves

NOTES:

Fluorescence yield and open & closed PSII reaction centers

Falkowski & Raven (1997) Figure 3.11

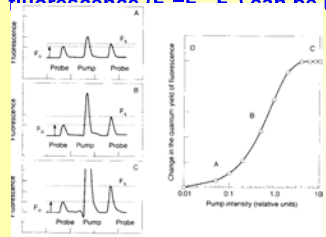


Slide 14 Fluorescence yield and open & closed PSII reaction centers

NOTES:

F_o , minimal Chl a fluorescence (dark fluorescence)

Falkowski & Raven (1997): Pump intensities close PSII reaction centers. F_o & differences in fluorescence ($F_o - F$) can be used to estimate

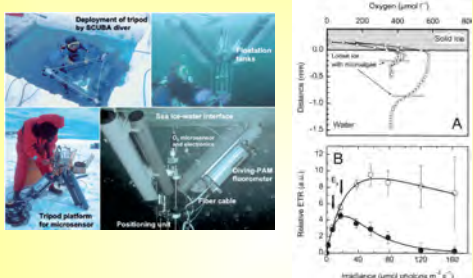


Slide 15 F_o , minimal Chl a fluorescence (dark fluorescence)

NOTES:

PAM Fluorometer & O₂ microsensor

Kühl et al. 2002 MEPS 223: 1-14

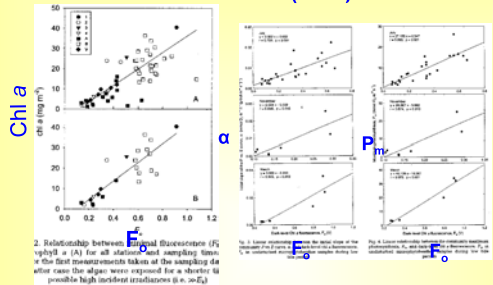


Slide 16 PAM Fluorometer & O₂ microsensor

NOTES:

F_o linearly related to Chl a, α, & P_{max}

Barranquet & Kromkamp (2000), Serôdio & Catarino (2000)

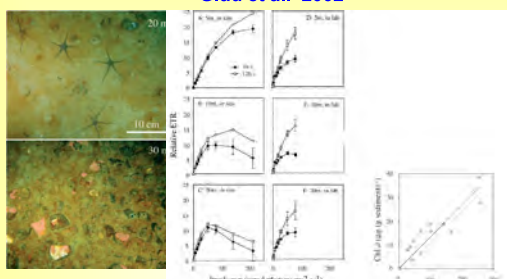


Slide 17 F_o linearly related to Chl a, α, & P_{max}

NOTES:

Measuring Production using fluorescence by SCUBA

Glud et al. 2002

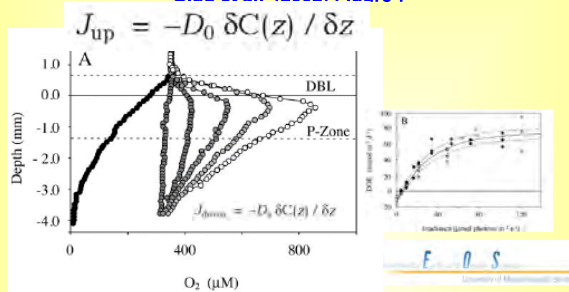


Slide 18 Measuring Production using fluorescence by SCUBA

NOTES:

Comparing production using fluorescence & O₂ flux by SCUBA

Glud et al. (2002) Figure 7

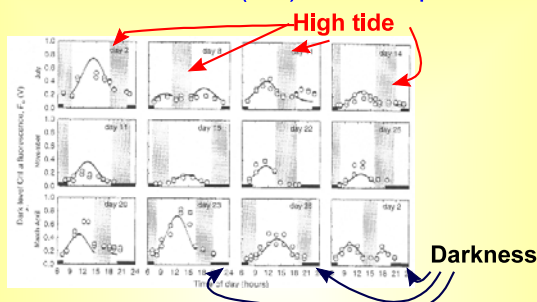


Slide 19 Comparing production using fluorescence & O₂ flux by SCUBA

NOTES:

Modeled effects of tide & light

Serôdio & Catarino (2000) Estimates of production



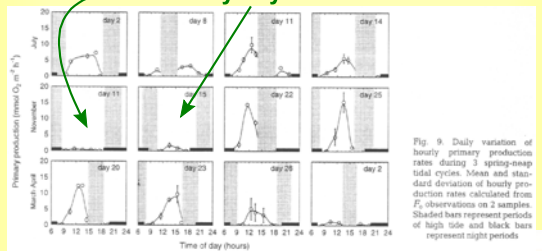
Slide 20 Modeled effects of tide & light

NOTES:

Modeled effects of tide & light

Serôdio & Catarino (2000)

Cloudy days



Slide 21 Modeled effects of tide & light

NOTES:

Rates of diatom production

Epipelagic: about 100-200 gCm⁻²y⁻¹

Location/Source	Technique	g C/m ² /y*	Author
Benthic microalgae:			
Georgia salt marsh	O ₂ , CO ₂	200	Potter (1959)
Diked salt marsh	O ₂	38-99	Gallagher and Daiber (1973)
California salt marsh	O ₂	217-400	Zedler (1980)
Massachusetts salt marsh	¹⁴ C (shaded)	106	Van Raalte et al. (1976)
Intertidal sandflat	radioactive	155	
Intertidal sandflat	O ₂	143-226	Fanamhat (1969)
Intertidal sandflat	O ₂	0.3-1.0	Holland and Phillips (1972)
Intertidal sandflat	¹⁴ C	4-9	Schoepf and Hedges (1983)
Intertidal mudflat	¹⁴ C	31	Leach (1970)
Estuarine subtidal	¹⁴ C	116	Grossart (1980)
Estuarine subtidal	¹⁴ C	99	Marchant (1970)
Wadden Sea sand flat	¹⁴ C	180	Jouet (1978)
Wadden Sea sand flat	¹⁴ C	58-177	Cadée (1980)
Sea and marsh grasses:			
Thalassia beds	O ₂	520-640	Westlake (1963)
Species (USA)	O ₂	257-350	Reed (1971)
(North Carolina to Nova Scotia)	cropping	130-256	Mann (1972b)
(Massachusetts)	cropping	1100-2300 ^a	Valeika et al. (1976)
Mangrove example:			
Florida (est prod.)	O ₂ (+ litter)	400	Mann (1972b)
Kelp:			
Laminaria (Nova Scotia) (England)	cropping	1900	Westlake (1963)
(Nova Scotia)	blade renewal	1225	Bateman et al. (1968)
(Mediterranean)	cropping	1750	Mann (1972b)
Littoral seagrass:			
Perse	O ₂	<3000 ^b	Kawatscher (1966)

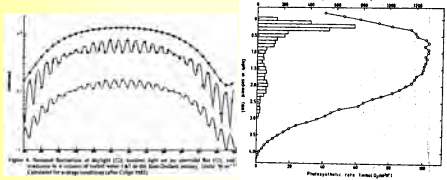
Slide 22 Rates of diatom production

NOTES:

What limits benthic production?

Light in winter, DIC in summer

- Production limited by light in winter
- Production may be limited by inorganic carbon in North temperate mudflats throughout the remainder of the year

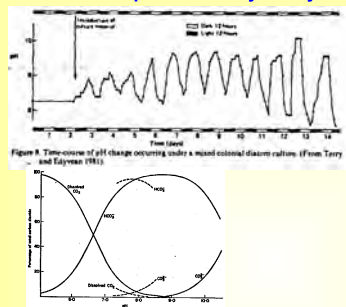


Slide 23 What limits benthic production?

NOTES:

DIC limitation in diatoms mats

pH from Terry & Edyeave (1981)



Slide 24 DIC limitation in diatoms mats

NOTES:

pH & species composition

N. salinarum replaced by *N. pygmaea*

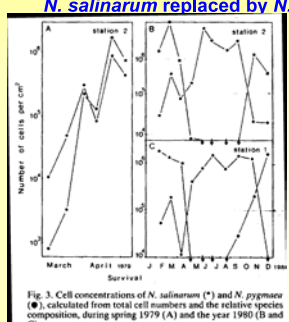


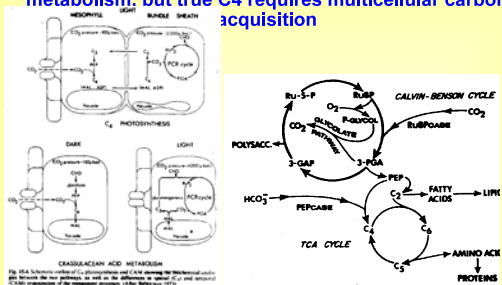
Fig. 3. Cell concentrations of *N. salinarum* (*) and *N. pygmaea* (●), calculated from total cell numbers and the relative species composition, during spring 1979 (A) and the year 1980 (B) and C).

Slide 25 pH & species composition

NOTES:

Acclimation to low DIC

C3 & C4 photosynthesis; diatoms have a C4-like DIC metabolism, but true C4 requires multicellular carbon acquisition



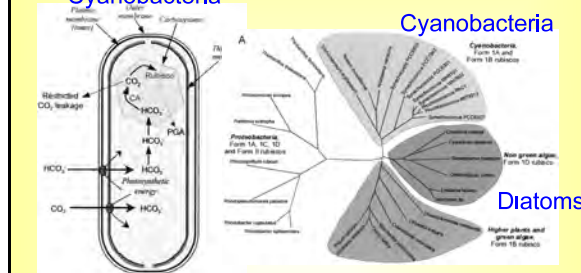
Slide 26 Acclimation to low DIC

NOTES:

Evolutionary History of DIC Concentrating mechanisms

Badger & Price (2003) Figs 1 & 2

Cyanobacteria



Slide 27 Evolutionary History of DIC Concentrating mechanisms

NOTES:

Cyanobacterial evolution & DIC concentrations; the end of nature?

Badger & Price (2003) Figs. 7 & 8

The diagram illustrates the evolution of cyanobacteria and their impact on Earth's environment. It shows the timeline from 3600 to 0 million years before present. Key events include the origin of cyanobacteria around 2500 MYA, the rise of oxygen levels (~20% O2) around 2000 MYA, and the appearance of eukaryotes around 1000 MYA. The Paleoproterozoic Eon (2.5-1.6 Ga) is labeled as the 'Great Oxidation Event'. The Neoproterozoic Eon (1.6-0.6 Ga) includes the 'Great Oxygenation Event' and the 'Great Dying' at the Permian-Triassic boundary. The Phanerozoic Eon (0.6-0 Mya) is shown with the Cambrian explosion and the rise of land plants. The ROD (Rockstratigraphic GEOLCARB III) model is used to predict future CO2 levels.

Slide 28 Cyanobacterial evolution & DIC concentrations; the end of nature?

NOTES:

Microphytobenthos: dominates benthic food supply

Slava Epstein's White Sea food web

The food web diagram shows energy flow from microphytobenthos (green arrow) through dinoflagellates and diatoms to various consumers including Harpacticoid copepods, H. ulvae, M. balthica, lug worms, ciliates, ostracods, and turbellaria. Bacteria are also shown as a source of energy for some organisms.

ECOS630

Slide 29 Microphytobenthos: dominates benthic food supply

NOTES:

Herman et al. 2000

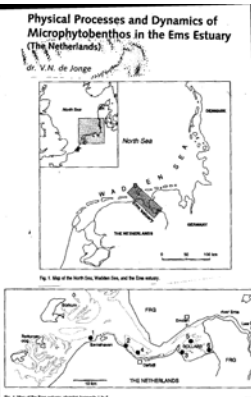
Linear relation between microphytobenthic production and infaunal biomass

A scatter plot showing the relationship between microphytobenthic production (mg C m⁻² h⁻¹) on the x-axis and infaunal biomass (g ADW m⁻²) on the y-axis. The data points show a strong positive linear correlation.

Fig. 8. Relation between microphytobenthic primary production (Herman et al., 1988, C. 1990) and infaunal biomass (dry weight). Infaunal biomass was calculated to be directly dependent on microphytobenthos (MPB) (see Table 2 for parameters and 'Discussion' for calculation). Linear correlation coefficient is 0.91 ($n = 5$, $p = 0.034$). ADW: ash-free dry wt.

Slide 30 Herman et al. 2000

NOTES:



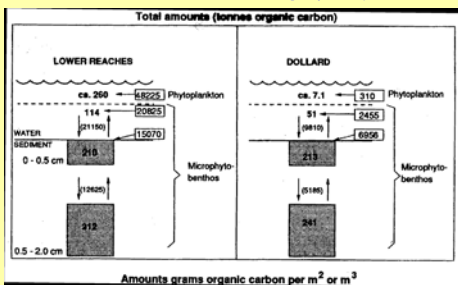
ECOS630

Slide 31

NOTES:

Photoautotrophic standing stock

From de Jonge (1994)



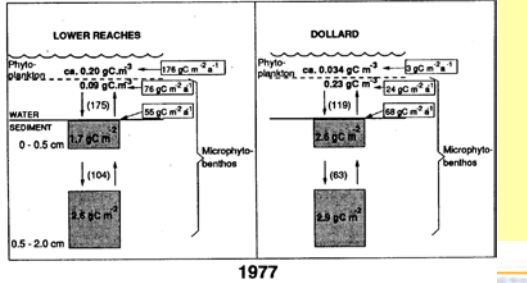
Slide 32 Photoautotrophic standing stock

NOTES:

Photoautotrophic production

From de Jonge

Amounts grams organic carbon per m² or m³



Slide 33 Photoautotrophic production

NOTES:

<p>Microphytobenthos & phytoplankton</p> <ul style="list-style-type: none">● Ems Dollard<ul style="list-style-type: none">▶ Microphytobenthic production $60\text{-}250 \text{ mgC m}^{-2} \text{ d}^{-1}$▶ 30% of phytoplankton are resuspended microphytobenthos● Dollard (about 1 m deep)<ul style="list-style-type: none">▶ 92% of Chl a from microphytobenthos▶ Production<ul style="list-style-type: none">■ 25% of total production from resuspended benthic diatoms■ 53% from true phytoplankton■ 22% from tidal flat production  <p>University of Massachusetts Boston</p>	<p>Slide 34 Microphytobenthos & phytoplankton</p> <p>NOTES:</p> <p> </p> <p> </p> <p> </p> <p> </p> <p> </p>
---	---